Anchoring of actin to the plasma membrane enables tension production in the fission yeast cytokinetic ring

Shuyuan Wang[a] and Ben O'Shaughnessy[b,*]
[a]Department of Physics and [b]Department of Chemical Engineering, Columbia University, New York, NY 10027

ABSTRACT **The cytokinetic ring generates tensile force that drives cell division, but how tension emerges from the relatively disordered ring organization remains unclear. Long ago, a musclelike sliding filament mechanism was proposed, but evidence for sarcomeric order is lacking. Here we present quantitative evidence that in fission yeast, ring tension originates from barbed-end anchoring of actin filaments to the plasma membrane, providing resistance to myosin forces that enables filaments to develop tension. The role of anchoring was highlighted by experiments on isolated fission yeast rings, where sections of ring became unanchored from the membrane and shortened ~30-fold faster than normal. The dramatically elevated constriction rates are unexplained. Here we present a molecularly explicit simulation of constricting partially anchored rings as studied in these experiments. Simulations accurately reproduced the experimental constriction rates and showed that following anchor release, a segment becomes tensionless and shortens via a novel noncontractile reeling-in mechanism at about the velocity of load-free myosin II. The ends are reeled in by barbed end–anchored actin filaments in adjacent segments. Other actin anchoring schemes failed to constrict rings. Our results quantitatively support a specific organization and anchoring scheme that generate tension in the cytokinetic ring.**

Monitoring Editor
Alex Mogilner
New York University

Received: Mar 27, 2019
Revised: May 31, 2019
Accepted: May 31, 2019

INTRODUCTION

Cytokinesis is the final stage of the cell cycle, when cells assemble an actomyosin contractile ring that constricts the cell into two (Pollard and O'Shaughnessy, 2019). The basic mechanical function of the ring is to generate tension, and hence to exert inward force that drives cell cleavage. Ring tensions of 10–50 nN were reported in echinoderm embryos (Rappaport, 1967, 1977; Yoneda and Dan, 1972; Hiramoto, 1975) and of ~400 pN in protoplasts of the fission yeast *Schizosaccharomyces pombe* (Stachowiak *et al.*, 2014), but the mechanism that produces tension has not been established.

How do the molecular components coordinate to generate tension in the ring? Following its discovery, and the finding that actin and myosin II are major components, the parallels with muscle were compelling and a musclelike sliding filament mechanism was proposed (Schroeder, 1972; Fujiwara and Pollard, 1976; Mabuchi and Okuno, 1977). However, contractile rings appear relatively disordered, and evidence for the highly ordered architecture of muscle based on the sarcomere repeat unit is lacking (Green *et al.*, 2012; Laplante *et al.*, 2015). A second, conceptually simple possibility is that ring tension derives from passive elasticity, using principles similar to those governing elastic fibers in the extracellular matrix (Kielty *et al.*, 2002). In this picture the ring behaves like a stretched elastic band whose tension depends only on its length.

A third possible mechanism, consistent with the disorder seen in contractile rings, is based on the anchoring of individual actin filaments to the plasma membrane by their barbed ends. No sarcomeric organization or permanent cross-linking between actin

This article was published online ahead of print in MBoC in Press (http://www.molbiolcell.org/cgi/doi/10.1091/mbc.E19-03-0173) on June 19, 2019.
The authors declare no competing financial interests.
Author contributions: B.O'S. conceived the study; B.O'S. and S.W. designed the model; S.W. performed the simulation; B.O'S. and S.W analyzed the data; B.O'S. and S.W. wrote the manuscript.
*Address correspondence to: Ben O'Shaughnessy (bo8@columbia.edu).
Abbreviation used: 3D, three-dimensional.

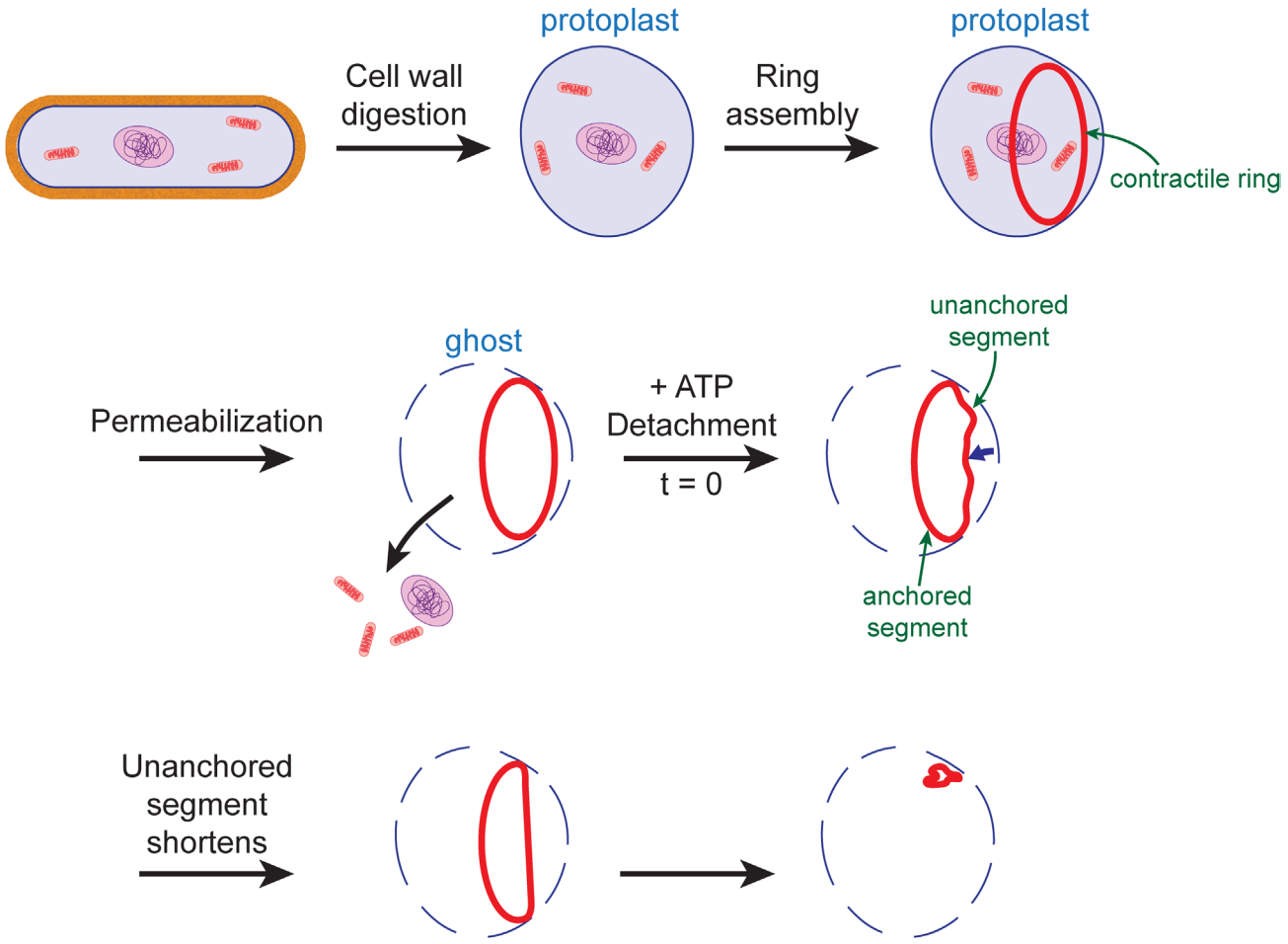

FIGURE 1: Schematic of cytokinetic ring constriction observed in permeabilized fission yeast protoplasts by Mishra *et al.* (2013). Protoplasts were generated from normal intact yeast cells by digestion of the cell wall, a fraction of which assembled cytokinetic rings. The plasma membrane was then permeabilized by detergent treatment so that cytoplasm escaped, resulting in cell ghosts that contained isolated contractile rings, lacking the highly viscous cytoplasm and its constituents. On addition of ATP, in a typical sequence a segment of ring detached from the weakened membrane and then shortened at ~30× the normal constriction rate until it became straight. While the unanchored segment shortened, the anchored segment remained of fixed length. Subsequent detachment and shortening sequences complete ring constriction. Note that during the shortening and straightening episode the unanchored segment is dragged through the aqueous medium, whose viscosity is presumably far less than that of the cytoplasm.

filaments is involved. Rather, overlapping filaments randomly positioned around the ring are independently made tense by myosin II that binds and pulls each filament. The net ring tension is the sum of such independent filament contributions. This mechanism of tension production in individual filaments was demonstrated during assembly of the ring of the fission yeast *S. pombe*, when anchored myosin -II pulls barbed end–anchored actin filaments and renders them tense to draw together the node precursors of the ring (Vavylonis *et al.*, 2008). Superresolution studies suggest that anchoring of actin-filament barbed ends to the plasma membrane persists in constricting fission yeast rings (Laplante *et al.*, 2016), and further support is provided by molecularly detailed simulations of constricting fission yeast rings that reproduce experimentally measured ring tensions (Stachowiak *et al.*, 2014; O'Shaughnessy and Thiyagarajan, 2018; Pollard and O'Shaughnessy, 2019).

This last mechanism requires firm lateral anchoring of barbed ends to the membrane to oppose the myosin force and allow the filament to become tense. If anchoring were compromised, the ring tension would be severely impacted. The effect of anchor loss was examined by Mishra *et al.* (2013) in an experimental study of fission yeast cell ghosts, permeabilized cells that lack cytoplasm and provide a unique laboratory for studying isolated cytokinetic rings. On addition of ATP, entire sections of rings became unanchored by pulling away from the plasma membrane (Figure 1). Subsequently, the unanchored segments shortened until they became taut, whereas anchored segments did not visibly contract. The shortening rate of the unanchored segments, 0.22 ± 0.09 μm s^{-1}, was ~30-fold the normal constriction rate and was independent of initial ring length.

The findings of Mishra *et al.* (2013) are unexplained, and the implications for the ring tension mechanism are not established. Here, we mathematically model constriction of partially anchored cytokinetic rings, comparing the predictions with a series of measurements reported in Mishra *et al.* (2013). We begin with a simple argument to show that these experimental findings are inconsistent with either a passive elastic or a sarcomeric musclelike tension mechanism. We then develop a molecularly detailed mathematical model of the fission yeast ring, which shows that the results of Mishra *et al.* (2013) are in quantitative agreement with the barbed end–anchoring tension hypothesis. The model shows that tensionless unanchored segments shorten by a novel noncontractile "reeling-in"

mechanism and accurately reproduces the observed shortening rate, which is identified as the load-free velocity of myosin II.

RESULTS

Experimental shortening rates of unanchored ring segments are inconsistent with elastic or sarcomeric tension mechanisms

In the experiments of Mishra *et al.* (2013), segments of contractile rings in fission yeast ghosts became unanchored from the plasma membrane. The unanchored segments had a typical initial radius of curvature R ~2 μm and were pulled with velocity v ~200 nm s^{-1} through the cell ghost aqueous contents as they shortened (Figure 1). As the cytoplasm is removed in ghosts, the expected viscosity of the aqueous medium is similar to that of water, ν_{water} = 0.001 Pa·s. Thus the drag coefficient per unit length of a typical ring segment of length L ~2 μm and thickness w ~0.2 μm (Stachowiak *et al.*, 2014) is ~$4\pi\nu_{water}/[\ln(2L/w) - 0.31]$ ~ 10^{-3} pN s/μm^2 (Broersma, 1960). Balancing viscous drag and tensile forces, $T/R \sim \zeta v$, yields a negligible tension, $T \sim 2 \times 10^{-3}$ pN, some five orders of magnitude smaller than the ~400 pN reported experimentally (Stachowiak *et al.*, 2014).

Thus, unanchored segments have essentially zero tension. This conclusion is inconsistent with a passive elastic mechanism, since an elastic ring segment would retain its tension even when unanchored, similarly to an elastic band whose ends are held in place at the two locations where the unanchored segment joins the anchored segment. Further, the shortening rate was independent of the initial length of the unanchored segment (Mishra *et al.*, 2013), inconsistent with a sarcomeric mechanism, for which the rate would be proportional to the number of unanchored sarcomeres, n_{sarc}, and hence the initial segment length. Indeed, the experimental shortening rate is of order the load-free myosin-II velocity, ~v^0_{myo}, whereas we find that an unanchored sarcomeric ring segment would shorten much more rapidly, at ~$n_{sarc}\, v^0_{myo}$ (see below).

Model of the fission yeast cytokinetic ring and its application to partially anchored rings

If unanchored ring segments have zero tension, why do they shorten? And why is the shortening rate ~0.22 μm s^{-1}, ~30-fold the normal rate? To address these issues quantitatively, we developed a molecularly detailed three-dimensional (3D) simulation of the *S. pombe* cytokinetic ring anchored to the inside of the plasma membrane, Figure 2. The *S. pombe* ring is particularly well characterized, as the amounts and biochemical properties of many contractile ring proteins were measured (Wu and Pollard, 2005; Arasada and Pollard, 2014; Goss *et al.*, 2014), severely constraining the model. Thus, we were able to determine all of the model parameters from previous experimental measurements, with no free parameters (see Supplemental Note S1 and Supplemental Table S1 for model details and parameters).

In the model, formin-capped actin filaments (Kovar *et al.*, 2006) are anchored to the membrane at their barbed ends (Laplante *et al.*, 2016), while anchored myosin II clusters (Schroeder and Otto, 1988; Naqvi *et al.*, 1999) exert force according to the force–velocity relation for myosin II (Edman, 1979), binding and pulling actin filaments dynamically cross-linked by α-actinin dimers (Figure 2A).

The lateral mobilities of the formin and myosin anchors in the membrane, γ_{myo} and γ_{for}, were previously determined from measurements of the velocity of each component in live cells (Stachowiak *et al.*, 2014). The values of γ_{myo} and γ_{for}, are of order 1 nN s/μm (see Supplemental Table S1). Given typical lipid diffusivities D_{lipid} ~1–10 μm^2/s (Almeida *et al.*, 2005), it follows that γ_{myo} and γ_{for} are ~6 orders of magnitude greater than the drag coefficient of a single lipid in the membrane, $\gamma_{lipid} = kT/D_{lipid}$. This is because formin Cdc12 and myosin II molecules in the ring appear to belong to substantial membrane-anchored protein complexes whose lateral mobility within the membrane is far less than that of a single lipid. A similar situation pertains during the ring assembly phase, when formins and myosin II belong to membrane-anchored protein complexes called nodes with reported drag coefficients γ_{node} ~0.2 nN s/μm (Vavylonis *et al.*, 2008), similar in magnitude to γ_{myo} and γ_{for}. Note that such high values of γ_{myo} and γ_{for} are critical to the tension mechanism described above that is based on anchoring of actin filaments to the membrane; were the drag coefficients an order of magnitude smaller, for example, the anchors would offer such little resistance to myosin forces that the ring tension would be negligible (Stachowiak *et al.*, 2014).

The model is fully 3D and dynamic. The ring can follow any contour in space, and detailed positions and configurations of components are represented over the ring cross-section and along its length (Figure 2). Actin filaments, for example, can orient in any direction and assume any 3D shape, determined by the forces exerted upon them and the known bending stiffness of F-actin. Crowding effects are accounted for by interactions between components. Component motions are tracked in all directions; for example, when a ring segment detaches from the membrane, the components experience forces tending to pull them away from the membrane through the aqueous medium, while viscous drag forces from the medium oppose this motion (Figures 1 and 2B). The model can describe fast component motions and high constriction rates, essential to capture the 30-fold normal constriction rates in cell ghosts. The model autonomously constricts the ring, as the ring length is continuously updated according to the evolving component locations.

We used the model to simulate constriction of partially unanchored rings in permeabilized protoplasts (Figures 1 and 2B). We begin with a normal steady state ring, an ~0.2 μm–wide bundle of randomly positioned myosin II clusters and actin filaments oriented parallel to the ring with random polarity, consistent with experiment and simulations of fully anchored rings (Stachowiak *et al.*, 2014; Supplemental Note S1). At time $t = 0$, the myosin II and formin anchors are removed in a segment of the ring, mimicking an initial detachment episode following ATP addition (Mishra *et al.*, 2013). As most cytoplasmic constituents are absent in cell ghosts (Mishra *et al.*, 2013), binding of new components (Pelham and Chang, 2002; Yonetani *et al.*, 2008; Stachowiak *et al.*, 2014) is absent. Dissociation rates were determined from the experimentally measured loss in component amounts in ghosts over the course of constriction and are considerably reduced from normal (Mishra *et al.*, 2013; Supplemental Table S1).

The basic computational method is as follows (for details, see Supplemental Note S1). The actin filaments are represented by chains of beads. Myosin clusters and formin dimers are represented by beads. At each time step, component velocities and actin filament tensions in the unanchored segment of the ring are computed by balancing aqueous medium viscous drag forces with myosin II and other forces, subject to the constraint that the distance between each actin subunit along a filament remains fixed. A similar force balance is applied to the anchored region, but formin Cdc12 dimers and myosin II clusters are constrained to move within the surface of the membrane and additionally experience membrane anchor drag forces. Once all forces and velocities are determined, the positions of individual ring components are updated using the Euler method with a time step $\Delta t = 1$ ms. At every time step, a number of randomly selected formin dimers, myosin II clusters, and α-actinin cross-links are removed from the simulation, and a number of randomly selected actin segments are severed, to reproduce the dissociation

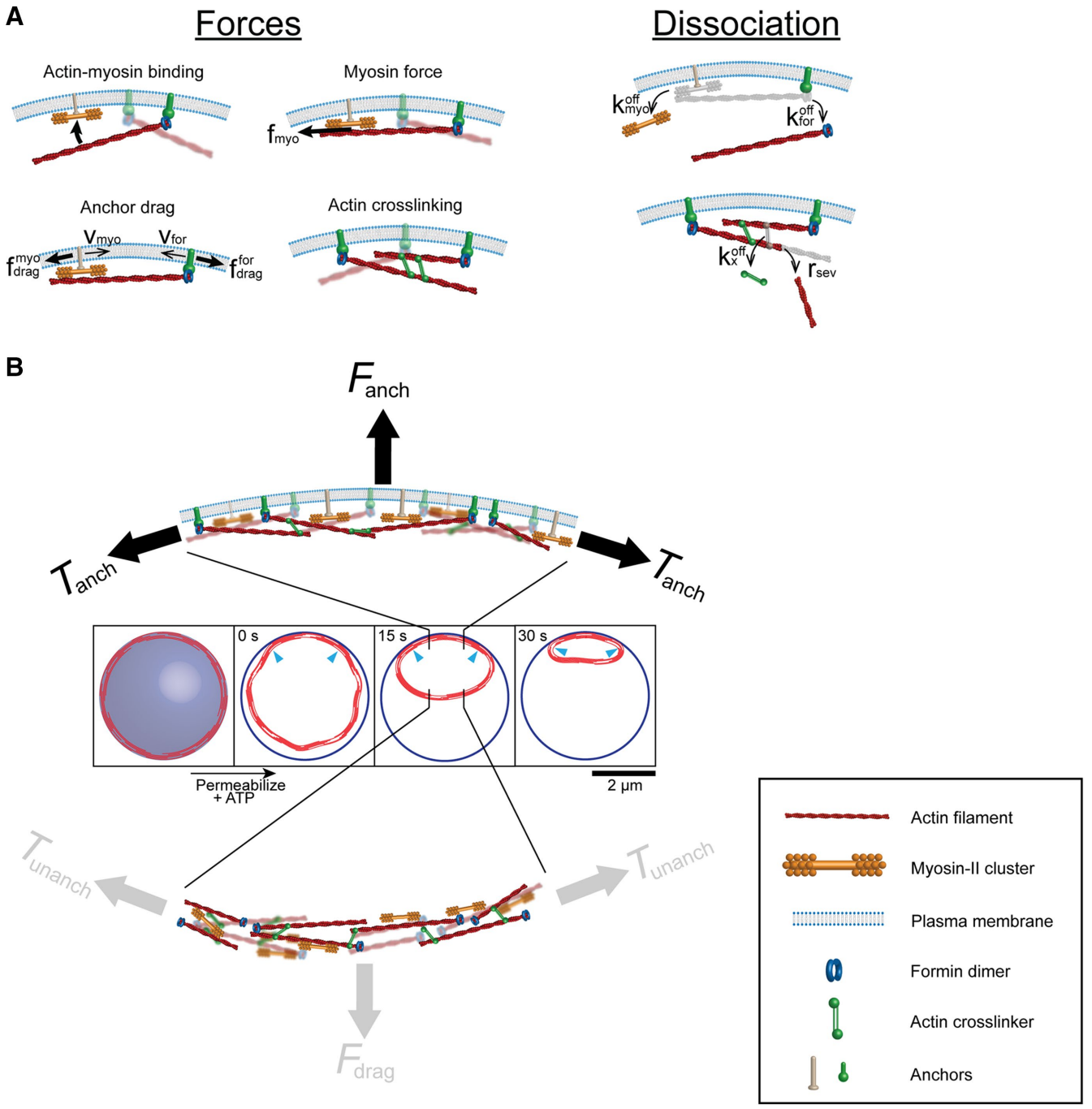

FIGURE 2: Barbed end–anchored 3D model of the cytokinetic ring in permeabilized fission yeast protoplasts (components not to scale). For component amounts and parameters see Supplemental Note S1 and Supplemental Table S1. (A) Actin filaments, membrane-anchored by formin Cdc12p, bind membrane-anchored myosin II that pulls actin following a linear force-velocity relation. Anchors move laterally, resisted by membrane drag forces, while drag from the aqueous medium acts on moving actin, myosin II, and formin. These components dissociate without replenishment, since these permeabilized cells lack cytoplasm (Mishra *et al.*, 2013). Simulations were run without α-actinin cross-linkers, as they dissociated within ~2 s; simulated constriction rates were unaffected (Supplemental Figure S2). Actin dissociates by unbinding with formins and by stochastic cofilin-mediated filament severing. (B) Constriction of a partially unanchored ring. Initial ring lengths 12–19 μm (Mishra *et al.*, 2013). The initially anchored ring is a disordered bundle (Stachowiak *et al.*, 2014). At t =0 s (ATP addition), partial detachment is simulated by removal of anchors in a segment and a small displacement. Depicted ring shapes are from a simulation with an initial ring 17 μm long and 80% unanchored. The unanchored segment shortens, not the anchored segment. Arrowheads: anchored/unanchored interfaces. Top: a portion of the anchored segment (schematic). The ring tension T_{anch} balances the net force from anchors that attach components to the membrane, F_{anch}. Bottom: In the unanchored segment, components can move in any direction. The ring tension is negligible, $T_{unanch} \ll T_{anch}$, because it balances a tiny net drag force from the aqueous medium, F_{drag}.

and severing rates inferred from Mishra *et al.* (2013). The ring tension is computed by summing actin filament tensions over the cross section.

Unanchored ring segments in simulations are tensionless

Using initial ring lengths of 12–19 µm (Mishra *et al.*, 2013), we compared simulated ring shapes, constriction rates, and tensions with experiment (Mishra *et al.*, 2013). In a typical simulated tension profile 1 s after detachment (Figure 3A), the tension is negligible in the unanchored segment, but substantial in the anchored segment.

In the anchored segment, the tension peaked at a mean value of 342 ± 51 pN (n = 10), similarly to the experimentally reported ~390 pN for normally anchored rings (Stachowiak *et al.*, 2014). With time, tension in the anchored segment decreased due to component dissociation and incoming actin filaments that saturated anchored myosin II clusters (Figure 3B).

Thus, the model reproduces the almost vanishing tension of unanchored ring segments in experiments. The origin of the anchoring requirement for tension is apparent from the ~0.5 pN force that myosin II clusters exerted on barbed end–anchored actin filaments they interacted with in the anchored region (Figure 3C), sustained by large anchor drag forces (10.7 ± 5.0 pN at 10 s, n = 321 filaments in 10 simulated rings). This created tension in the slowly moving filaments. By contrast, the unanchored segment was tensionless because myosin slid unanchored actin filaments at close to the load-free velocity, v^0_{myo}, working against almost zero drag force (Figure 3C).

The model reproduces experimental constriction rates that are independent of ring length

In simulations, in agreement with experiment, the unanchored segments shortened, but not the anchored segments. The simulated constriction rates were remarkably close to the experimental values. Despite being tensionless, simulated unanchored segments shortened until they became almost straight after ~25–60 s (Figures 2B and 3, D and E, and Supplemental Movie S1). The shortening rate was independent of the initial length of ring or unanchored segment, and approximately constant in time, with a mean time average 0.24 ± 0.05 µm s^{-1} (n = 47) (Figure 3, E–I). Anchored segments scarcely shortened (~3% shortening, Supplemental Movie S2). These results reproduce the observations of Mishra *et al.* (2013), where only unanchored segments shortened and the constriction rate, 0.22 ± 0.09 µm s^{-1}, was consistent over many cells with rings of variable initial length.

Unanchored ring segments are noncontractile and are reeled in at their ends

Remarkably, the shortening of unanchored ring segments was not contractile, as revealed by the constant separation between fiducial markers in simulated constricting rings (Figure 4A). One might imagine that the rapid shortening of tensionless unanchored segments is driven by a contraction mechanism working against zero load, similar to zero load muscle contraction (Edman, 1979). On the contrary, these segments shortened by being *reeled in* at their two ends where they joined the anchored segment. Each end was reeled in at about half the myosin-II load-free velocity, ~0.5 v^0_{myo}, the mean velocity with which myosin entered the anchored segment (Supplemental Figure 4, B and E, and Supplemental Movie S3), giving a net shortening rate ~v^0_{myo} . The noncontractile shortening left the myosin density in the unanchored segment constant in time and approximately spatially uniform (Figure 4, A and C), while reeled-in myosin accumulated in puncta of growing amplitude near the anchored/unanchored interfaces (Figure 4, A, arrowheads, and C).

Rings constrict at close to the load-free velocity of myosin II in permeabilized protoplasts

It is noteworthy that for both simulations and experiments the constriction rates are of order the myosin II load-free velocity in our simulations, v^0_{myo} = 0.24 µm s^{-1} (Supplemental Table S1). We stress that this is an experimental value, taken from Stark *et al.* (2010) where v^0_{myo} was measured in *S. pombe* rings versus number of myosin-II (Myo2p) molecules per actin filament which we set to 20 from the ratio of Myo2p to formin Cdc12p molecules measured in the ring in Wu and Pollard (2005) (Supplemental Note S1). That the constriction rate could be related to v^0_{myo} is plausible, because unanchored segments encounter negligible viscous drag force while shortening. To test this, we artificially varied v^0_{myo} through the range 0.01–0.5 µm s^{-1}. Simulations showed that the constriction rate (1.07 ± 0.09) × v^0_{myo} can indeed be identified as a constant times v^0_{myo} over a large range (Figure 3J).

Reeling in is caused by barbed end–anchored actin filaments

What causes reeling in, and why is the shortening rate close to v^0_{myo}? We found that reeling in is a direct consequence of the barbed-end anchoring of actin filaments that is the basis of tension generation in normally anchored rings. The agents of reeling in are actin filaments in the interfacial zone whose barbed ends are anchored to the membrane in the anchored segment (Figure 5C). About half of these filaments straddled the interface, their pointed ends oriented into the unanchored segment (Supplemental Note S1 and Supplemental Figure S1). These filaments grabbed unanchored myosin II clusters and reeled in the unanchored segment at the load-free myosin velocity v^0_{myo}, as the segment offered negligible load due to the low viscosity of the medium in cell ghosts. This process occurs at both ends, suggesting a net shortening rate ~2 v^0_{myo}. In practice, the rate ~v^0_{myo} is somewhat lower (Figure 3, I and J), due to sliding resistance from anchored myosin clusters on incoming actin filaments and myosin crowding at the interface (Figure 4 and Supplemental Note S1).

Other actin-anchoring schemes cannot reproduce the experiments

That the model reproduces the experimental length-independent shortening rate of ~v^0_{myo} strongly supports the specific actin-anchoring scheme assumed, at or near barbed ends. Other anchoring schemes cannot explain the experiments: with pointed-end or midfilament anchoring, actin filaments at the anchored/unanchored interface are wrongly oriented, and simulations failed to constrict unanchored segments (Figure 5, D and E). For example, with pointed-end anchoring, those anchored filaments that straddle the interface are oriented with barbed ends extending into the unanchored segment; because myosin II migrates toward barbed ends, the unanchored ring segment tends to get pushed out rather than contract. With midfilament anchoring, both orientations occur equally often (barbed or pointed ends, respectively, extending into the unanchored ring segment) so that contractile and expansive forces cancel.

Constricting rings in permeabilized protoplasts have three distinct zone types

Thus, partially anchored rings have three distinct zone types (Figure 5, A and B). 1) In the anchored region, anchored myosin clusters interacting with randomly oriented anchored actin filaments have a low net velocity (Figure 4B), giving a very low shortening rate. 2) The unanchored segment is a freestanding random actomyosin bundle. As drag forces are negligible, myosin works against zero load, generates no contractility or tension, and

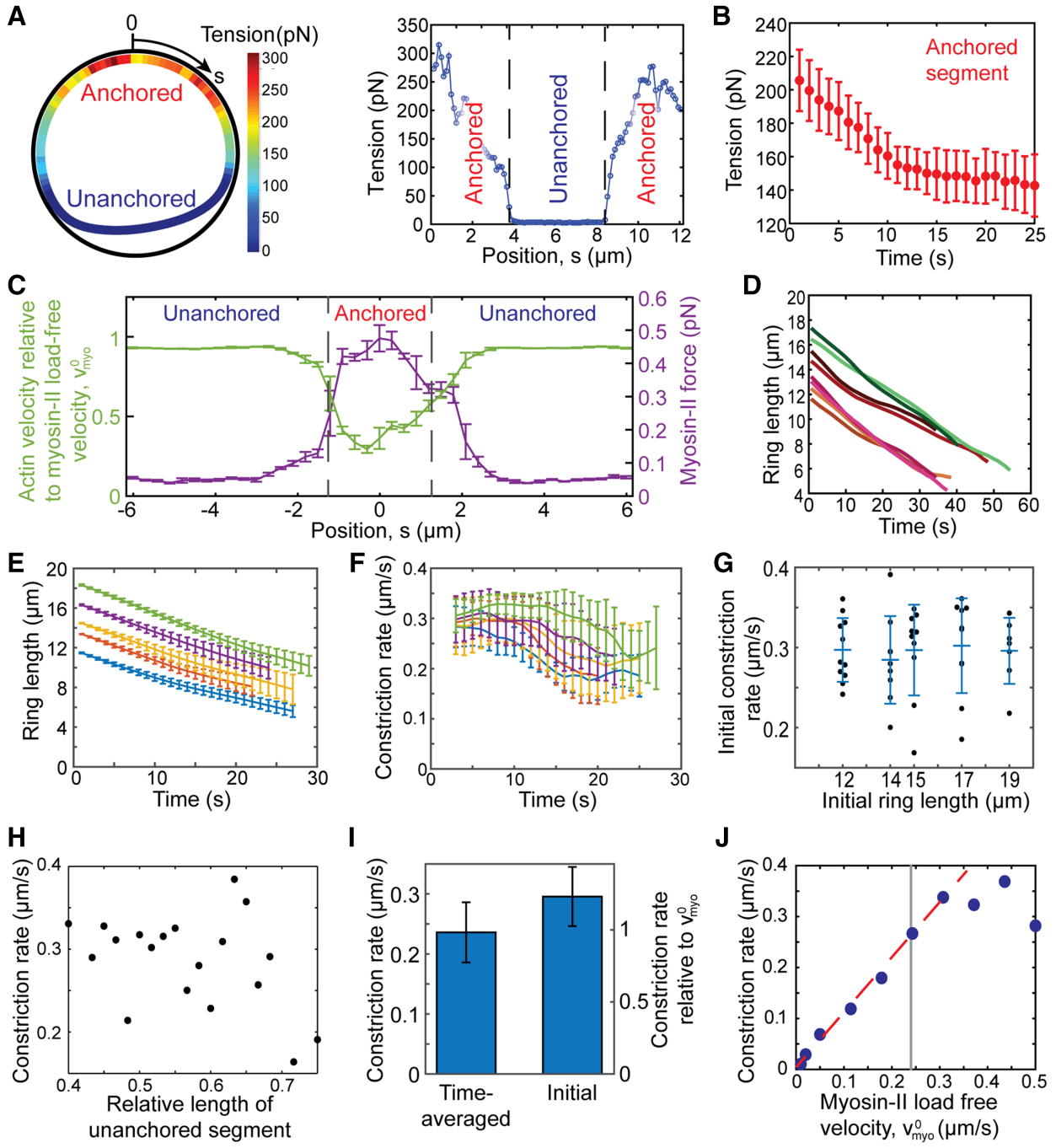

FIGURE 3: Unanchored ring segments have zero tension and constrict at close to the load-free velocity of myosin II, v^0_{myo}, independent of initial length. Simulations of partially unanchored rings. Initial length 12.6 μm, unanchored segment 20% of ring length, unless otherwise stated. For other parameters, see Supplemental Note S1 and Supplemental Table S1. Error bars: SD. (A) Tension in a simulated ring 1 s after detachment of a segment 40% of ring length. Anchoring is required for ring tension. The unanchored segment has almost zero tension. (B) Tension vs. time in the anchored segment ($n = 10$ simulations). Forty percent of ring initially unanchored. (C) Actin filament velocities relative to the myosin II clusters they interact with (green) and mean forces exerted by myosin II clusters per actin filament they interact with (purple). Mean values over a length of 0.3 μm, one simulation. (D) Length of partially unanchored ring vs. time for eight simulations; initial length 12–18 μm. (E) Length of partially unanchored ring vs. time for initial lengths 12, 14, 15, 17, and 19 μm averaged over $n = 11$, 9, 10, 10, and 7 simulations, respectively. (F) Mean constriction rates (rates of decrease of ring length) vs. time for constrictions of E. (G) The initial constriction rate is independent of initial ring length ($p = 0.96$, one-way analysis of variance). Constriction rates from E at 1 s. Bars: mean ± SD. (H) The time-averaged constriction rate and initial length of unanchored segment relative to total ring length are uncorrelated (correlation coefficient $r = –0.40$, $p = 0.094$, $n = 19$ rings). (I) Time-averaged and initial constriction rates averaged over all constrictions of E, $n = 47$. (J) In simulations with a range of v^0_{myo} values, the time-averaged constriction rate was ~1.07 v^0_{myo} over most of the range (95% confidence interval: 0.98 v^0_{myo} – 1.16 v^0_{myo}, least-squares fit of first seven points, dashed line). Gray line: value used throughout this study (0.24 μm s^{-1}).

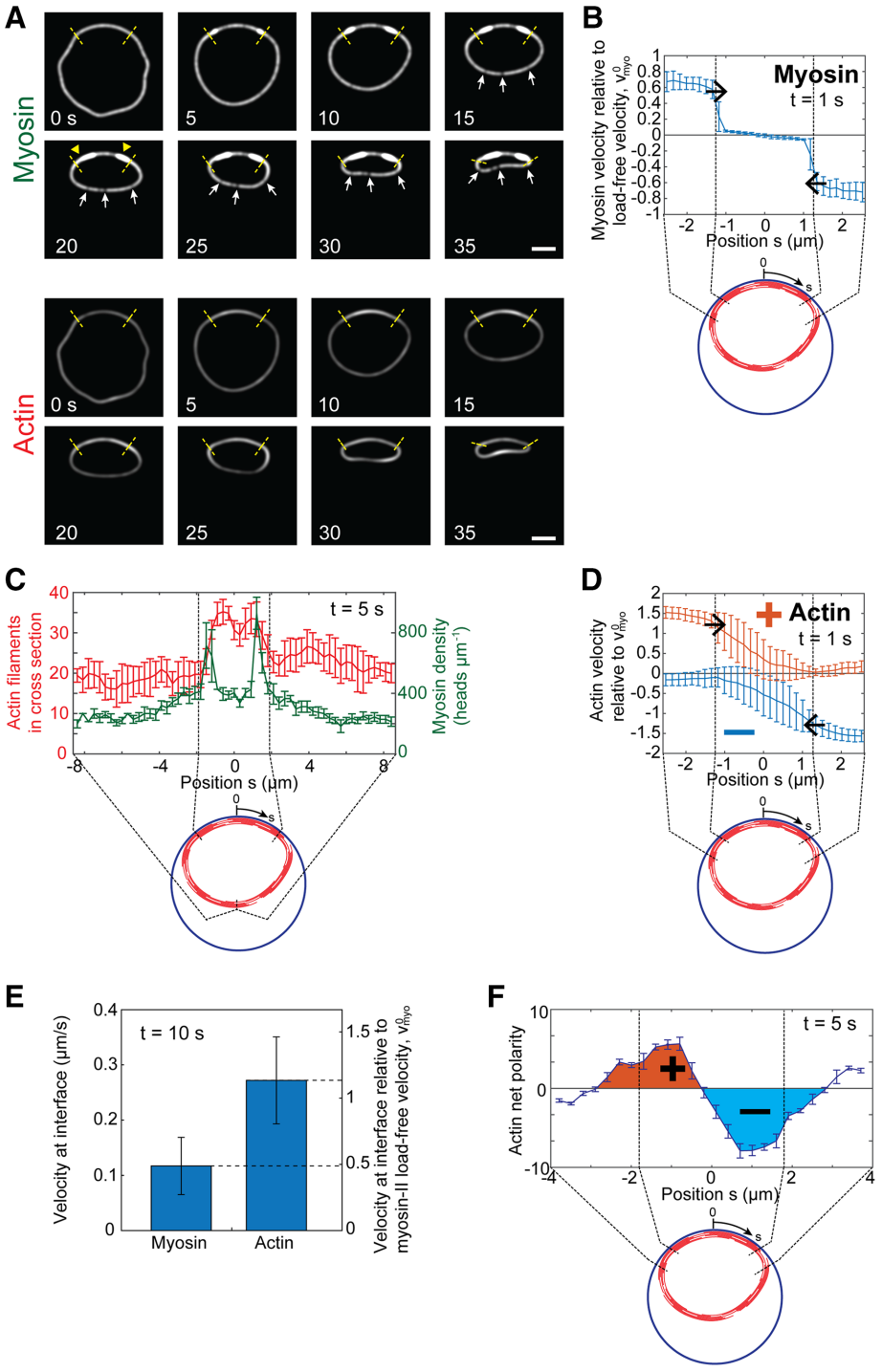

FIGURE 4: Unanchored ring segments are noncontractile and shorten by being reeled in at close to the myosin II load-free velocity, $v^0_{myo} = 0.24$ μm s^{-1}. Simulation parameters as for Figure 3 unless otherwise stated. Error bars: SD. (A) Simulated time-lapse images of the constricting ring of Figure 2B, with fluorescently tagged myosin II and actin. Shortening of the unanchored segment is noncontractile: fiducial markers have constant separation (arrows), and myosin and actin densities remain constant. Instead, the unanchored segment is reeled in so that myosin II accumulates in puncta (arrowheads) near the anchored/unanchored interfaces (dashed lines). The anchored segment does not shorten. Fluorescence imaging simulated with a 2D Gaussian point spread function, width 200 nm, centered on myosin II clusters or actin subunits. (B) Velocity profiles of myosin II in the interfacial and anchored zones after 1 s. Unanchored myosin II enters the anchored segment with velocity ~0.5 v^0_{myo}, the reeling-in velocity. Mean velocities parallel to the ring, averaged over bin size 1/6 μm and 10 simulations. (C) Myosin and actin density profiles 5 s after partial detachment. Myosin puncta develop near each interface and actin accumulates in the anchored segment. Both densities are approximately uniform in the unanchored segment. Mean densities, averaged over a bin size 0.3 μm and $n = 7$ rings, initial length 19 μm. (D) Velocity profile of actin subunits belonging to clockwise-oriented (+) and counterclockwise-oriented (–) filaments in the interfacial and anchored zones after 1 s. Unanchored filaments of a definite polarity enter the anchored region at each end, with velocity ~1.1 v^0_{myo} (E) Mean velocities of incoming unanchored myosin II and actin as the components enter the anchored region, time 10 s. The myosin velocity, ~0.5 v^0_{myo}, is the reeling-in velocity. The actin velocity, ~1.1 v^0_{myo}, is less than v^0_{myo} greater than the myosin velocity due to sliding resistance from anchored myosin clusters and interfacial crowding. Mean values over a region within 0.1 μm of the interface (60 myosin-II clusters, 543 actin subunits, 10 simulations). (F) Net actin polarity (number of clockwise- minus counterclockwise-oriented filaments) in the interfacial and anchored zones in simulations of C. Clockwise (counterclockwise) polarity bias develops near the left (right) interface.

propels actin filaments with velocity v^0_{myo} clockwise or anticlockwise (depending on polarity) that enter the anchored segment with a velocity ~v^0_{myo} greater than the myosin reeling-in velocity (Figure 4, D and E). These filament motions leave the actin density unaffected, except for the latest stages (Figure 4, A and C), and produce net polarity puncta in the interfacial zones (Figure 4F). 3) In the interfacial zones, noncontractile reeling in occurs (Figure 5A).

Anchoring is required for ring constriction

The simulations showed that anchoring is required not only for tension, but also for ring constriction. Entirely unanchored simulated rings had almost vanishing tension and did not constrict (Figure 6, A and B, and Supplemental Movie S4), consistent with the images in Mishra *et al.* (2013) of constricting rings that featured at least one anchored segment. This is because reeling in of an unanchored segment requires the presence of an adjacent anchored segment whose barbed end–anchored actin filaments execute the reeling in. Actin-filament anchoring is the key requirement, as constriction occurred even without myosin anchoring in the anchored segment (Figure 6, A and B, and Supplemental Movies S5 and S6).

Dependence of fission yeast myosin II activity on ATP concentration

The load-free velocity, v^0_{myo}, is a fundamental molecular property of myosin II. We next

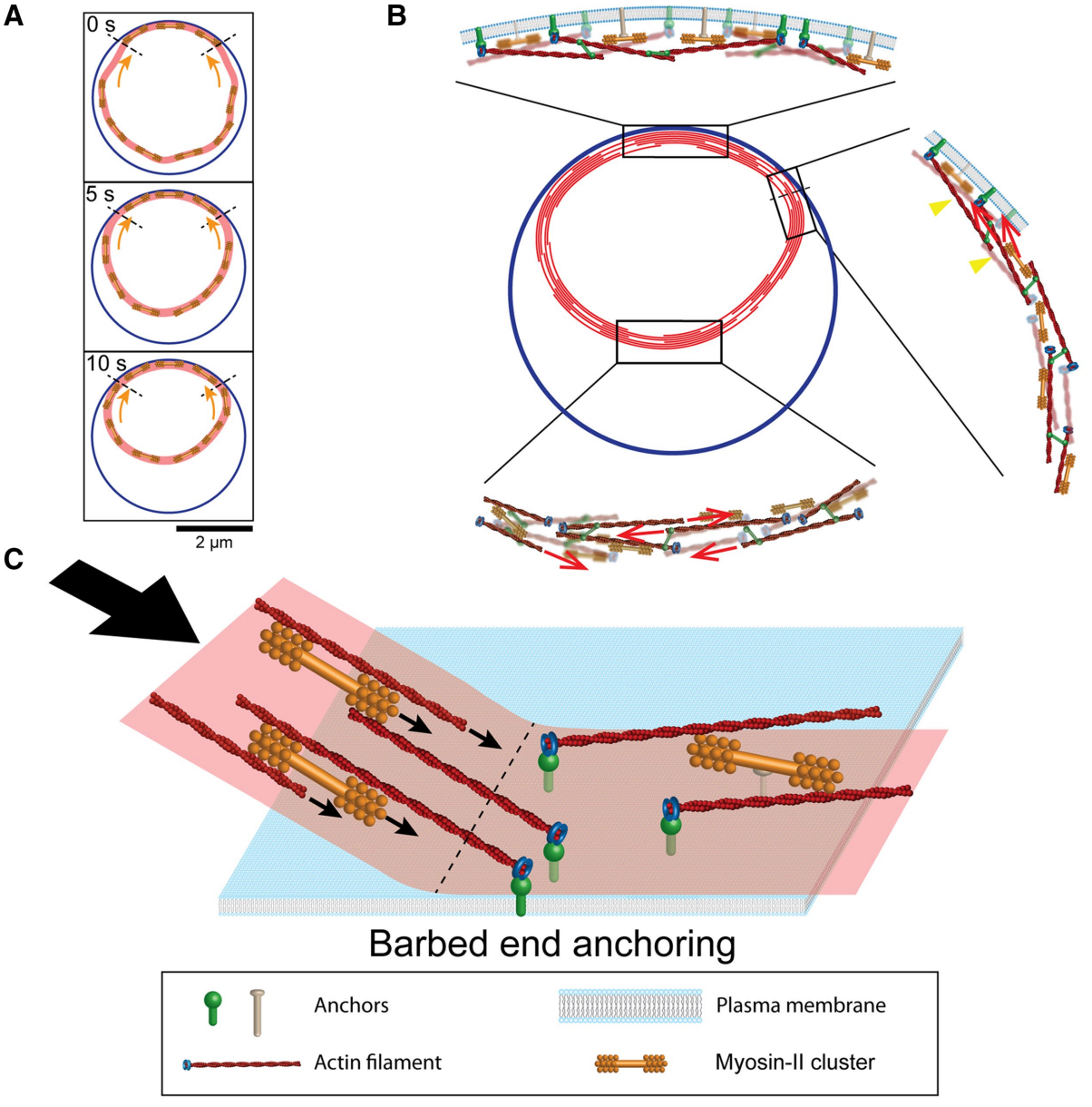
A
0 s
5 s
10 s
2 μm
B
C
Barbed end anchoring
Anchors
Plasma membrane
Actin filament
Myosin-II cluster
D
Pointed end anchoring
Mid-filament anchoring
E
Constriction rate (μm/s)
0.3
0.2
0.1
0
-0.1
-0.2
***
***
***
Barbed end
Near barbed end
Mid-filament
Pointed end
Anchoring scheme

used our simulations to infer the ATP dependence of v^0_{myo} for fission yeast from the measurements by Mishra *et al.* (2013) of constriction rate versus ATP concentration (blue points, Figure 7). The link between the two, provided by the simulations, is the dependence of constriction rate on v^0_{myo} (Figure 3J). Fitting to Michaelis–Menten kinetics yielded a maximal load-free velocity at saturating ATP of 0.23 μm s^{-1}, close to the 0.24 μm s^{-1}reported in Stark *et al.* (2010), and a half-maximal load-free velocity at 30 μM ATP (Supplemental Note S2). These values are in the context of the cytokinetic ring machinery, and we note that v^0_{myo} is a collective molecular property reflecting the complexities of the contractile ring architecture and interactions. For comparison, a half-maximal value of 50 μM ATP was measured in vitro for skeletal muscle myosin (Kron and Spudich, 1986). Related in vitro measurements in fission yeast were performed in Pollard *et al.* (2017), where the ATPase rate of fission yeast myosin Myo2 was measured versus actin concentration at saturating ATP levels.

Ring constriction in permeabilized protoplasts does not require actin turnover

It has been proposed that ring constriction is driven by actin depolymerization (Mendes Pinto *et al.*, 2012). To test this, Mishra *et al.* (2013) used a cofilin mutant or the F-actin–stabilizing drug jasplakinolide. Constriction rates were unaffected. To mimic these experiments, we ran simulations with cofilin-mediated severing abolished or reduced. In agreement with experiment, constriction rates were unaltered (Figure 6, C and D).

This finding is as expected, because in the reeling-in mechanism the constriction rate is set by v^0_{myo}, which is unaffected by the lengths of actin filaments in the ring. Hence, no dependence of constriction rate on cofilin or other actin polymerization/depolymerization factors is expected. Thus, our model explains why actin turnover is not required for constriction of partially unanchored rings.

DISCUSSION

The cytokinetic ring occupies center stage during cytokinesis, and its ability to generate tension and constrict is critical to cell division. How it produces tension remains unsettled, in part because many organizational details are unknown. Evidence for musclelike sarcomeric machinery is lacking, although some superresolution microscopy and electron microscopy images show a degree of spatial periodicity of the organization in animal cells (Beach *et al.*, 2014; Fenix *et al.*, 2016; Henson *et al.*, 2017). The ring organization appears to exhibit considerable randomness (Green *et al.*, 2012; Laplante *et al.*, 2015), so that the mechanism appears something of a puzzle, given that a theoretical actomyosin bundle with randomly organized actin filaments and myosin II is not tensile (Lenz *et al.*, 2012). Indeed, our simulations of freestanding randomly organized actomyosin rings produced no tension (Figure 6).

Our analysis showed that the experiments of Mishra *et al.* (2013) provide quantitative evidence that fission yeast solves this problem simply by anchoring actin filaments at their barbed ends to the membrane in the ring. Conceptually, this is a natural way to create tension out of disorder, as every myosin–actin interaction renders the filament involved tensile (Figure 6E). (Compare this with the random, unanchored bundle, where dynamically cross-linked myosin-propelled actin filaments are as often tensile as compressive.) The net ring tension is the sum effect of these tensile filament contributions without the need for a particular organization, sarcomeric or other.

Here we built a model implementing this organization, which quantitatively reproduced the observations of Mishra *et al.* (2013): 1) unanchored ring segments had zero tension (Figure 3A) 2) with no fitting parameter segments shortened at close to the zero-load velocity of myosin II, with mean rate 0.24 μm s^{-1} very close to the experimental value 0.22 μm s^{-1} (Figure 3), and 3) the shortening rate was independent of initial length (Figure 3G). Anchoring schemes other than barbed-end anchoring could not explain these findings (Figure 5, C and D).

The experimental observations, 1–3, are inconsistent with a passive elastic mechanism, which would generate tension in an unanchored segment, or with a sarcomeric-like organization of interconnected contractile units, which would shorten at a rate proportional to the number of sarcomeric units and initial length. In *Caenorhabditis elegans* embryos, for example, shortening rates in successive divisions are proportional to initial ring length, not inconsistent with a sarcomerelike organization (Carvalho *et al.*, 2009). In contrast, length-independent shortening, 3), is a hallmark of the reeling-in mechanism we identified (Figure 5), which acts at the ends of an

FIGURE 5: Reeling-in mechanism of ring constriction in permeabilized protoplasts. (A) Unanchored ring segments are reeled in at their ends. The simulated ring of Figure 2B is shown at the indicated times. Reeling in (arrows) at the interface with the anchored segment (dashed lines) is not contractile, so that on average the distance between myosin II clusters remains constant (myosin II clusters shown schematically, not to scale). (B) The three distinct zones of simulated partially anchored rings. In the unanchored segment (bottom), almost stationary myosin clusters propel actin filaments at the zero load velocity v^0_{myo} (arrows) clockwise or counterclockwise, depending on filament polarity. Components have much lower velocities in the anchored segment (top), due to viscous drag forces from component anchors in the plasma membrane. In the interfacial region (right), actin filaments and myosin clusters are reeled into the anchored segment at velocities of order v^0_{myo} (arrows) by anchored actin filaments that bridge the interface and orient into the unanchored segment (arrowheads). (C) The reeling-in mechanism relies on barbed-end anchoring of actin filaments to the plasma membrane. Filaments lie parallel to the ring, randomly oriented clockwise or counterclockwise. Thus, about half of the filaments anchored close to the anchored/unanchored interface (dashed line) straddle the interface, with their pointed ends oriented into the unanchored segment. These filaments grab unanchored myosin clusters and reel in the unanchored ring segment against almost zero load. This figure was adapted from Pollard and O'Shaughnessy (2019). (D) Pointed-end or midfilament actin anchoring schemes do not constrict rings in permeabilized protoplasts. With pointed-end anchoring, actin filaments straddling the interface have the wrong orientation for reeling in, since myosin II migrates to actin-filament barbed ends. Instead, the unanchored segment is pushed outward. Midfilament anchoring produces zero net reeling in, as filaments of both orientations straddle the interface. (E) Simulated constriction rates for different anchoring schemes. Only anchoring at or near barbed ends constricts rings, and only barbed-end anchoring reproduces the experimental constriction rate of 0.22 μm s^{-1}. Mean constriction rates, time-averaged over 20 s (or until ring fracture, for pointed-end anchoring) and over $n = 10$ simulations. Model parameters as for Figure 3. Error bars: SD. ***$p < 0.01$.

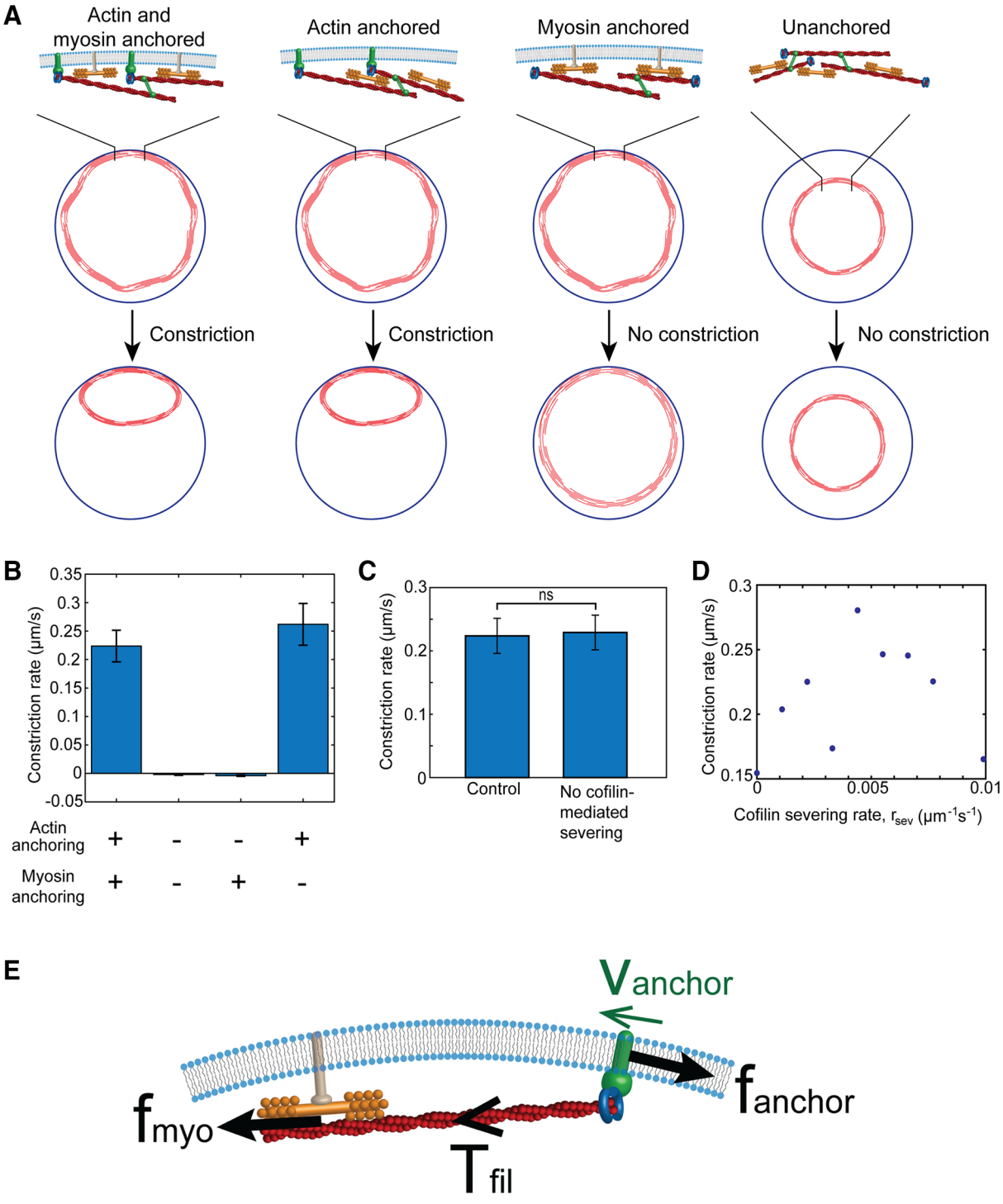

FIGURE 6: Constriction of cytokinetic rings in permeabilized protoplasts requires anchoring of actin but not actin turnover. Simulation results, model parameters as in Figure 3. Constriction rates are from linear fits to simulated ring lengths vs. time. (A, B) Partially anchored rings constrict when both actin and myosin are anchored or when only actin is anchored. Loss of actin anchoring abolishes constriction, either for rings with only myosin anchored in the anchored segment (elongation rate 4 ± 1 nm s^{-1}) or for completely unanchored rings (elongation rate 2 ± 2 nm s^{-1}). Mean values shown, averaged over $n = 10$ (with actin anchoring) or $n = 13$ (without actin anchoring) simulations. Error bars: SD. (C) There is no statistically significant difference between constriction rates of rings with (control) and without cofilin-mediated severing of actin filaments. Simulations without severing mimic the addition of jasplakinolide in the experiments of Mishra *et al.* (2013). Error bars: SD. (D) Constriction rate vs. rate of cofilin-mediated severing of actin filaments. The constriction rate and severing rate are uncorrelated ($n = 9$, correlation coefficient $r = 0.17$, $p = 0.65$). (E) Schematic of anchoring mechanism for tension generation in the fission yeast contractile ring. A typical actin filament barbed end is anchored to the membrane via formin Cdc12p (blue) and a membrane anchor (green). The anchor moves laterally in the membrane when pulled by myosin-II, resisted by the drag force f_{anchor}. The myosin force and the resultant filament tension T_{fil} are substantial, provided the anchor velocity v_{anchor} is much less than the load-free myosin II velocity v^0_{myo}.

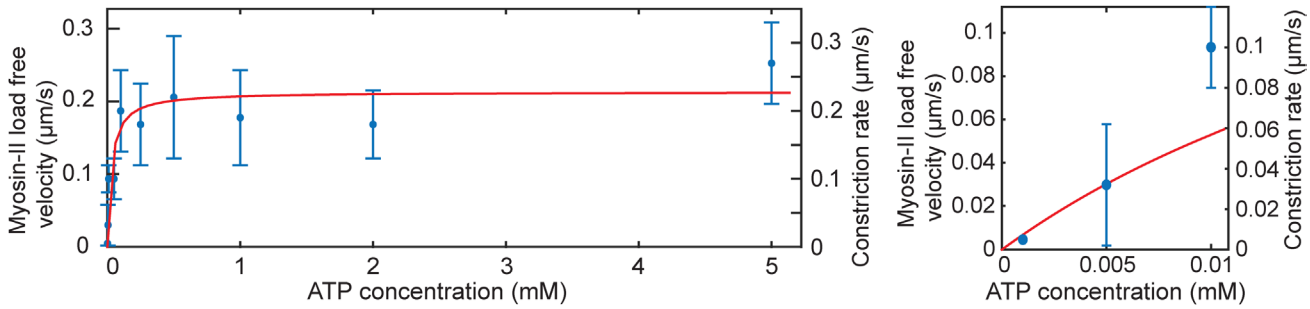

FIGURE 7: Myosin II load-free velocity and constriction rate vs. ATP concentration. Constriction rates are experimental values from Mishra *et al.* (2013). The corresponding myosin II velocities (i.e., the scale for the vertical axis at left) were obtained from the experimental constriction rates using the best-fit line in Figure 3J. Red curve: best-fit Michaelis–Menten relation, corresponding to a maximal load-free velocity at saturating ATP of 0.23 μm s^{-1} and a half-maximal load-free velocity at 30 μM ATP (Supplemental Note S2). Plot at right: blow-up near origin.

unanchored segment unaffected by the intervening segment length. In our simulations we also found no evidence for buckling of actin filaments, which was observed in reconstituted bundles and was shown theoretically to be able to generate tension in such bundles (Lenz *et al.*, 2012).

Thus, both radial and lateral anchoring feature in the contractile ring machinery. Radial anchoring attaches the ring to the membrane and conveys the ring tension to the membrane, the cortex, and, for fungi such as fission yeast, the cell wall. Lateral anchoring restrains lateral motion of ring components and features in the tension mechanism by retarding lateral sliding of actin-filament barbed-end anchors in the membrane, allowing the filaments to develop tension when pulled by myosin (Figure 6E). The requirement for tension is that the lateral sliding velocity be well below v^0_{myo}, a condition that is satisfied in fission yeast (Laplante *et al.*, 2016).

Overall, we emphasize that the chief conclusions of this study concern the contractile ring tension mechanism in normal cells under physiological cytokinesis conditions. Our main finding is that if the tension mechanism in *normal* fully anchored rings is that myosin II pulls membrane-anchored actin filaments (as depicted in Figure 6E), then in an *abnormal* ring with an unanchored segment, that segment would shorten at ~v^0_{myo} (the load-free myosin velocity). Thus, by confirming this predicted unanchored segment shortening rate, as well as a number of other predictions (see Supplemental Table S2), the experiments of Mishra *et al.* (2013) quantitatively support the barbed end–anchoring mechanism in normal rings.

Our study shows how the behavior of the ring in an extraordinary nonphysiological situation (having an unanchored segment, in this case) can help reveal mechanisms in normal physiological rings (fully anchored). Indeed, the predicted nonphysiological behavior is only consistent with a specific anchoring scheme in normal rings, where actin filaments are anchored to the plasma membrane at their barbed ends. Simulations of normal rings assuming other anchoring schemes did not generate the experimentally observed constriction behavior when a segment was forcibly unanchored (see Figure 5). With barbed-end anchoring, the model predicted a novel noncontractile constriction mode of the unanchored segment in which its ends were reeled in by the anchored segment.

An implicit assumption of the present analysis is that the unanchoring process does not leave myosin II and other core ring components behind in the membrane. In support of this assumption, detached ring segments remained intact and contained dynamic myosin II Rlc1p, showing that some or all of the F-actin and myosin-II pulled away intact from the plasma membrane. Moreover, in the images of Mishra *et al.* (2013), myosin fluorescence on the membrane is not apparent in the vicinity of detached ring segments.

As a contractile cellular machine, the cytokinetic ring presumably has a signature tension–constriction rate relationship, analogously to muscle (Edman, 1979) and other actomyosin systems. Most of this relationship is normally invisible outside a narrow physiological operating range, but yeast cell ghosts provide a laboratory for studying the contractile ring in extraordinary circumstances outside this window. This can reveal otherwise hidden aspects of the workings of the machinery.

In fission yeast, two extremes of behavior corresponding to two regions of the tension–constriction rate relation are now characterized. 1) In normal cells, the ring works against a high load, and therefore constricts very slowly compared with component turnover rates. As far as the tension-generating mechanism is concerned, the ring behaves as if it were of fixed length: the ring operates near the isometric (fixed-length) tension limit (Stachowiak *et al.*, 2014; Thiyagarajan *et al.*, 2015). Thus the ring sets the tension to the isometric value, the value at fixed ring length and an intrinsic property of the ring (Stachowiak *et al.*, 2014), and does not set the constriction rate. For example, in yeast protoplasts, rings constrict at increasing speeds as constriction progresses (Mishra *et al.*, 2012; Stachowiak *et al.*, 2014), showing that the constriction rate is not intrinsic to the ring. Indeed, in normal yeast cells, the constriction rate is the rate of septum closure, and experiment and modeling suggest that there is almost no influence from ring tension (Thiyagarajan *et al.*, 2015). 2) Here we studied the opposite extreme in cell ghosts: fast, load-free constriction of partially anchored ring segments. In the load-free limit, the tension vanishes, and the ring constricts via a novel reeling-in mechanism in which the ring itself sets the constriction rate. In this mode the constriction rate is now an intrinsic property of the ring, a multiple of the load-free myosin II velocity, v^0_{myo}.

MATERIALS AND METHODS

Methods and any associated references are described in Supplemental Note S1.

Code availability

All simulations in the paper were performed in MATLAB. The source code is available upon request.

Statistical analysis

Differences between groups were compared using an unpaired, two-tailed Student's *t* test unless otherwise specified.

ACKNOWLEDGMENTS

We thank Sathish Thiyagarajan and Harvey F. Chin for helpful discussions. Research reported in this publication was supported by the National Institute of General Medical Sciences of the National Institutes of Health under Award R01GM086731. The content is solely the responsibility of the authors and does not necessarily represent the official views of the National Institutes of Health.

REFERENCES

Almeida PF, Vaz WL, Thompson TE (2005). Lipid diffusion, free area, and molecular dynamics simulations. Biophys J 88, 4434–4438.

Arasada R, Pollard TD (2014). Contractile ring stability in *S. pombe* depends on F-BAR Protein Cdc15p and Bgs1p transport from the Golgi complex. Cell Rep 8, 1533–1544.

Beach JR, Shao L, Remmert K, Li D, Betzig E, Hammer JA 3rd (2014). Nonmuscle myosin II isoforms coassemble in living cells. Curr Biol 24, 1160–1166.

Broersma S (1960). Viscous force constant for a closed cylinder. J Chem Phys 32, 1632.

Carvalho A, Desai A, Oegema K (2009). Structural memory in the contractile ring makes the duration of cytokinesis independent of cell size. Cell 137, 926–937.

Edman KA (1979). The velocity of unloaded shortening and its relation to sarcomere length and isometric force in vertebrate muscle fibres. J Physiol 291, 143–159.

Fenix AM, Taneja N, Buttler CA, Lewis J, Van Engelenburg SB, Ohi R, Burnette DT (2016). Expansion and concatenation of nonmuscle myosin IIA filaments drive cellular contractile system formation during interphase and mitosis. Mol Biol Cell 27, 1465–1478.

Fujiwara K, Pollard TD (1976). Fluorescent antibody localization of myosin in the cytoplasm, cleavage furrow, and mitotic spindle of human cells. J Cell Biol 71, 848–875.

Goss JW, Kim S, Bledsoe H, Pollard TD (2014). Characterization of the roles of Blt1p in fission yeast cytokinesis. Mol Biol Cell 25, 1946–1957.

Green RA, Paluch E, Oegema K (2012). Cytokinesis in animal cells. Annu Rev Cell Dev Biol 28, 29–58.

Henson JH, Ditzler CE, Germain A, Irwin PM, Vogt ET, Yang S, Wu X, Shuster CB (2017). The ultrastructural organization of actin and myosin II filaments in the contractile ring: new support for an old model of cytokinesis. Mol Biol Cell 28, 613–623.

Hiramoto Y (1975). Force exerted by cleavage furrow of sea-urchin eggs. Dev Growth Differ 17, 27–38.

Kielty CM, Sherratt MJ, Shuttleworth CA (2002). Elastic fibres. J Cell Sci 115, 2817–2828.

Kovar DR, Harris ES, Mahaffy R, Higgs HN, Pollard TD (2006). Control of the assembly of ATP- and ADP-actin by formins and profilin. Cell 124, 423–435.

Kron SJ, Spudich JA (1986). Fluorescent actin filaments move on myosin fixed to a glass surface. Proc Natl Acad Sci USA 83, 6272–6276.

Laplante C, Berro J, Karatekin E, Hernandez-Leyva A, Lee R, Pollard TD (2015). Three myosins contribute uniquely to the assembly and constriction of the fission yeast cytokinetic contractile ring. Curr Biol 25, 1955–1965.

Laplante C, Huang F, Tebbs IR, Bewersdorf J, Pollard TD (2016). Molecular organization of cytokinesis nodes and contractile rings by super-resolution fluorescence microscopy of live fission yeast. Proc Natl Acad Sci USA 113, E5876–E5885.

Lenz M, Gardel ML, Dinner AR (2012). Requirements for contractility in disordered cytoskeletal bundles. New J Phys 14, 033037.

Mabuchi I, Okuno M (1977). The effect of myosin antibody on the division of starfish blastomeres. J Cell Biol 74, 251–263.

Mendes Pinto I, Rubinstein B, Kucharavy A, Unruh JR, Li R (2012). Actin depolymerization drives actomyosin ring contraction during budding yeast cytokinesis. Dev Cell 22, 1247–1260.

Mishra M, Huang Y, Srivastava P, Srinivasan R, Sevugan M, Shlomovitz R, Gov N, Rao M, Balasubramanian M (2012). Cylindrical cellular geometry ensures fidelity of division site placement in fission yeast. J Cell Sci 125, 3850–3857.

Mishra M, Kashiwazaki J, Takagi T, Srinivasan R, Huang Y, Balasubramanian MK, Mabuchi I (2013). In vitro contraction of cytokinetic ring depends on myosin II but not on actin dynamics. Nat Cell Biol 15, 853–859.

Naqvi NI, Eng K, Gould KL, Balasubramanian MK (1999). Evidence for F-actin-dependent and -independent mechanisms involved in assembly and stability of the medial actomyosin ring in fission yeast. EMBO J 18, 854–862.

O'Shaughnessy B, Thiyagarajan S (2018). Mechanisms of contractile ring tension production and constriction. Biophys Rev 10, 1667–1681.

Pelham RJ, Chang F (2002). Actin dynamics in the contractile ring during cytokinesis in fission yeast. Nature 419, 82–86.

Pollard LW, Bookwalter CS, Tang Q, Krementsova EB, Trybus KM, Lowey S (2017). Fission yeast myosin Myo2 is down-regulated in actin affinity by light chain phosphorylation. Proc Natl Acad Sci USA 114, E7236–E7244.

Pollard TD, O'Shaughnessy B (2019). Molecular mechanism of cytokinesis. Annu Rev Biochem 88, 661–689.

Rappaport R (1967). Cell division: direct measurement of maximum tension exerted by furrow of echindoerm eggs. Science 156, 1241–1243.

Rappaport R (1977). Tensiometric studies of cytokinesis in cleaving sand dollar eggs. J Exp Zool 201, 375–378.

Schroeder TE (1972). The contractile ring. II. Determining its brief existence, volumetric changes, and vital role in cleaving Arbacia eggs. J Cell Biol 53, 419–434.

Schroeder TE, Otto JJ (1988). Immunofluorescent analysis of actin and myosin in isolated contractile rings of sea-urchin eggs. Zool Sci 5, 713–725.

Stachowiak MR, Laplante C, Chin HF, Guirao B, Karatekin E, Pollard TD, O'Shaughnessy B (2014). Mechanism of cytokinetic contractile ring constriction in fission yeast. Dev Cell 29, 547–561.

Stark BC, Sladewski TE, Pollard LW, Lord M (2010). Tropomyosin and myosin-II cellular levels promote actomyosin ring assembly in fission yeast. Mol Biol Cell 21, 989–1000.

Thiyagarajan S, Munteanu EL, Arasada R, Pollard TD, O'Shaughnessy B (2015). The fission yeast cytokinetic contractile ring regulates septum shape and closure. J Cell Sci 128, 3672–3681.

Vavylonis D, Wu JQ, Hao S, O'Shaughnessy B, Pollard TD (2008). Assembly mechanism of the contractile ring for cytokinesis by fission yeast. Science 319, 97–100.

Wu JQ, Pollard TD (2005). Counting cytokinesis proteins globally and locally in fission yeast. Science 310, 310–314.

Yoneda M, Dan K (1972). Tension at the surface of the dividing sea-urchin egg. J Exp Biol 57, 575–587.

Yonetani A, Lustig RJ, Moseley JB, Takeda T, Goode BL, Chang F (2008). Regulation and targeting of the fission yeast formin cdc12p in cytokinesis. Mol Biol Cell 19, 2208–2219.